The influence of citric acid on the microstructure and magnetic properties of cobalt ferrite nanoparticles synthesized by hydrothermal method

Morteza Adibi[1] · S. Mohammad Mirkazemi[1] · S. Alamolhoda[1]

Abstract

Cobalt ferrite nanoparticles were synthesized by the citric acid-assisted hydrothermal method with the citric acid to metal ion molar ratio (C/M) 0.5, 1, and 1.5. Nanoparticles were characterized by X-ray diffraction (XRD), field emission scanning electron microscopy (FE-SEM), and vibrating sample magnetometer (VSM) techniques. The coarse cobalt ferrite particles are synthesized along with hematite impurities when using the routine hydrothermal method. However, the results showed that single-phase and uniform cobalt ferrite nanoparticles were formed in the presence of citric acid. The obtained results also revealed that by changing the C/M ratio from 0.5 to 1 and 1.5, the mean crystallite size and maximum magnetization were changed from 7.8, 4.7, and 7.3 nm and 50.3, 40, and 48.2 emu/g, respectively. Therefore, citrate acid concentration plays a significant role in the final properties of synthesized particles. Moreover, this parameter is a powerful tool for regulating the properties of nanoparticles. In addition, in this study, a mechanism for synthesis producer and role of the chelating agent concentration, based on the stability of the formed complexes during the synthesis process and its effect on the nucleation temperature, has been presented.

Keywords Cobalt ferrite nanoparticles · Citric acid to metal ion ratio · Hydrothermal · Citrate-metal ion complex

1 Introduction

Nowadays, magnetic nanoparticles are used in ferrofluids, nuclear magnetic resonance (NMR) imaging, biomolecule detectors, catalyst, bearings and dampers, drug delivery, pollutant removal or toxicity mitigation, hyperthermia, high-density recording device, and permanent magnet applications [1–5]. Among the spinel ferrites, cobalt ferrite has received considerable attention due to its moderate saturation magnetization, high coercivity, high Curie temperature, excellent chemical stability, biocompatibility, and very high cubic magnetocrystalline anisotropy [6–9].

Magnetic properties, purity, particle size distribution, morphology, and particle size, are the key factors for the considered application influenced by the method and conditions of synthesis. Based on this, different synthesis methods are being employed [10–12]. Cobalt ferrite nanoparticles can be synthesized with different methods such as microemulsion [13], co-precipitation [14], electrochemical [15], thermal decomposition [16], sol–gel [17], hydrothermal [18], sol–gel hydrothermal [19]. Among these methods, hydrothermal is a cost-effective and convenient method that yielded high purity, narrow particle size, and controlled morphology products. Besides, surfactants and chelating agents, such as CTAB, PVA, citric acid (CA), PVP, are used as growth control agents that inhabited particle growth or caused particular morphologies in the hydrothermal synthesis [20, 21]. The effects of citric acid [19, 22], PVA [23], and CTAB [24] addition on hydrothermal synthesis of cobalt ferrite nanoparticles were investigated earlier.

Citric acid concentration is an effective factor on the final properties of products synthesized via the CA-assisted hydrothermal method. In this regard, Jiang et al. [25] reported the effects of CA concentration on the α-NaYF$_4$ particle size. Di et al. [26] prepared TbPO$_4$ nanocrystals by the hydrothermal route and revealed the effect of CA: Tb ratio on morphology and particle size. Cho et al. [27]

✉ S. Mohammad Mirkazemi
  mirkazemi@iust.ac.ir

1   School of Metallurgy and Materials Engineering,
    Iran University of Science & Technology (IUST),
    Narmak, Tehran, Iran

showed that the CA concentration influenced ZnO nanoparticles' morphologies. Zahraei et al. [28] showed that the CA concentration affects the purity of the synthesized $Mn_{0.6}Zn_{0.4}Fe_2O_4$ nanoparticles. Behdadfar et al. [29] synthesized Fe_3O_4 nanoparticles, and results showed a certain amount of CA was required to obtain single phase. Saini et al. [30] prepared different phases of VO_2 by varying the vanadium to the CA molar ratio. Soo-Min Park and Chunghee Nam [31] synthesized different morphologies of WO_3 nanoparticles using different CA concentrations. However, up to our knowledge, there is no report that investigated the effect of the CA concentration on the hydrothermal synthesis of cobalt ferrite nanoparticles.

In this present work, cobalt ferrite nanoparticles were synthesized via a citric acid-assisted hydrothermal method, and the impact and role of citric acid to metal ion molar ratio, as a criterion of citric acid concentration, was investigated and discussed based on XRD, FE-SEM, FTIR, and VSM results.

2 Experimental section

2.1 Materials

Starting materials were iron (III) nitrate-nonahydrate (Fe $(NO_3)_3.9H_2O$, Merck No. 103883), cobalt (II) nitrate-hexahydrate ($Co(NO_3)_2.6H_2O$, Merck No. 102536), sodium hydroxide (NaOH, Merck No. 106482), and citric acid monohydrate ($C_6H_8O_7.H_2O$, Merck No. 100242). These reagents were used without any further purification.

2.2 Preparation of cobalt ferrite nanopowder

Cobalt ferrite nanopowder was prepared as follows: first, appropriate amounts of cobalt nitrate and iron nitrate (molar ratio 1:2) separately were dissolved in deionized water. Subsequently, appropriate amounts of citric acid (molar ratio of CA to metal ion 0.5, 1, and 1.5) were dissolved in deionized water and separately were added to cobalt and iron nitrates solutions and stirred for 2 h. After that, the cobalt-containing solution was added to the iron-containing solution and stirred for 3 h. In the next step, the pH value of the solution was adjusted to 12 by dropwise adding the sodium hydroxide solution. Then the obtained suspension was transferred into a 100-ml Teflon sailed autoclave and heated to 180 ℃ for 9 h. After being cooled to room temperature, the obtained precipitate was collected by centrifuge and external magnet and washed with deionized water several times until reaching neutral pH. Finally, the obtained black powder was dried at 110 ℃ for 3 h. By comparison, a sample was also synthesized without CA (C/M ratio0). The synthesized samples

at different CA to metal ion molar ratios 0, 0.5, 1, 1.5 were named as CM0, CM0.5, CM1, and CM1.5, respectively.

2.3 Characterization

Phase analysis of samples was performed by the X-ray diffractometer (XRD, Rigaku Ultima IV) using Cu K_{α} radiation and graphite monochromator. The mean crystallite size (MCS) of nanoparticles was calculated by using the Scherrer equation:

$$D = \frac{k\lambda}{\beta\cos\theta} \tag{1}$$

where β is the width of the diffraction peak at half-maximum intensity, λ is the X-ray wavelength, θ is diffraction angle, and k is a constant [32]. The morphology of nanoparticles was investigated by field emission scanning electron microscopy (FE-SEM, Tescan MiraII). Before the investigation, the powders were dispersed in the ethanol media by ultrasonication and dried on a slide. The size of one hundred particles in the FE-SEM micrographs were determined by the ImageJ software, and the particle size distribution graphs were drawn.

Magnetic properties of the samples were measured with the vibrating sample magnetometer (VSM, Meghnatis Daghigh Kavir, MDK6) at room temperature and the maximum applied field of ± 10 kOe. IR spectra were recorded by Fourier transform infrared spectrometer (FTIR, Shimadzu 8500) in the region 400–4000 cm^{-1}.

3 Results and discussion

The XRD results of synthesized samples are shown in Fig. 1 (CM0, CM0.5, CM1, and CM1.5 related to the C/M ratio of 0, 0.5, 1, and 1, respectively). The obtained diffraction peaks are well matched with standard patterns of cubic $CoFe_2O_4$ (JCDPS card no. 22-1086). The diffraction peaks located in $2\theta = 18.2°, 30.0°, 35.4°, 37.0°, 43.0°, 53.4°, 56.9°, 62.5°, 65.7°, 70.9°, 74.0°, 75.0°,$ and $78.9°$ are related to (111), (220), (311), (222), (400), (422), (511), (440), (531), (620), (533), (622), and (444) crystallographic planes of CF's cubic spinel structure. Also, in the presence of citric acid, no impurity phase peaks were detected. Nevertheless, in the absence of citric acid, hematite (α-Fe_2O_3, JCPDS card no. 33-0664) phase trace has been detected. In addition, cobalt ferrite's diffraction peaks became sharper and narrower, which indicates the increase in crystallinity and crystallite size.

Hematite and goethite impurities were observed in other researches, and the presence of these phases is attributed to the difference in hydrolysis rates of iron and cobalt cations

Fig. 1 XRD patterns of synthesized samples
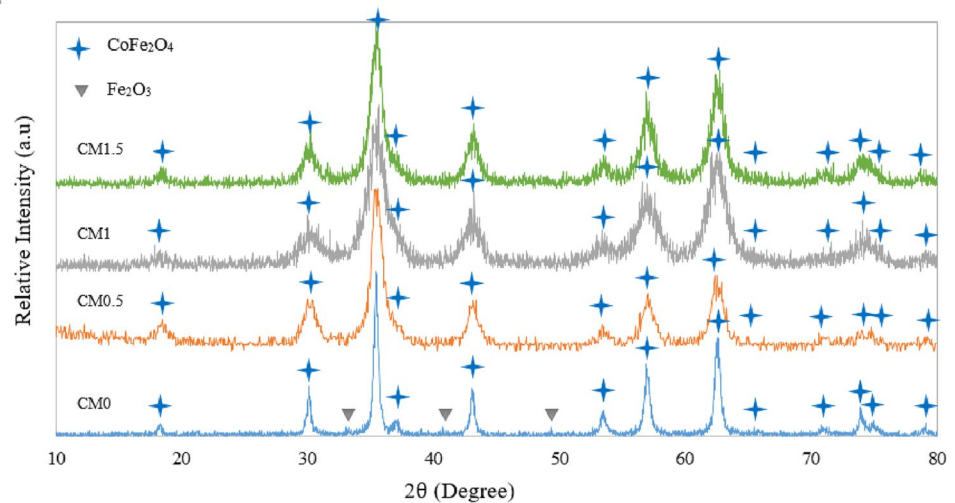
Table 1 Mean crystallite size of synthesized cobalt ferrite nanoparticle

Sample code	Crystallite size (nm)
CM0	21.3
CM0.5	7.8
CM1	4.3
CM1.5	7.3

[18]. During the hydrothermal process, first, the hydroxide and oxyhydroxide species are formed. In the next step, these species are converted to the oxide phase. Researches show that the hydrolysis constant of Fe^{3+} is higher than that of Co^{2+}, which means that the tendency of Fe^{3+} for hydroxide formation is higher than that of Co^{2+} [33]. This higher tendency during the reaction can lead to forming iron hydroxide-rich areas that are eventually converted into hematite. Also, one of the purposes and benefits of adding citric acid is to control the hydrolysis rate [34].

The average crystallite sizes were calculated from the most intense peak (311) by the Scherrer equation. The obtained results are presented in Table 1. The mean crystallite size of samples in C/M 0.5, 1, and 1.5 is 7.8, 4.7, and 7.3 nm, respectively. The mean crystallite size of CM1 is smaller than the other samples. The results confirm that different concentrations of citric acid have different effects and roles.

The proposed mechanism for citric acid-assisted hydrothermal included three main steps: (i) citrate-metal ion complex formation, (ii) decomposition of citrate-metal ion complexes and conversion to the metal hydroxide phases, (iii) conversion of metal hydroxide to the desired phase during the hydrothermal procedure [35, 36]. However, dissolution–crystallization is considered the primary mechanism of the hydrothermal process. The hydrothermal synthesis method consists of three main steps: (i) hydration ($Fe(OH)_3$,

$Fe(OH)_4^-$, $Co(OH)_2$, $Co(OH)_3^-$ formation), (ii) dehydration, (iii) nucleation and growth of oxide phase [37, 38]. The FTIR analysis was performed to ensure citric-metal complexes formed during the precursor preparation process. The IR spectra of the precursors (suspension obtained after the addition of sodium hydroxide to cobalt, iron, and citrate acid solution, before the hydrothermal treatment) are shown in Fig. 2. The absorption peaks at 1361 and 1591 cm^{-1} attributed to the asymmetric and symmetric stretching vibrations of carboxyl ions (COO^-) in the metal carboxylates, respectively, which confirmed the citrate-metal ion complex formation. Also, the absorption band at 622, 840, and 1155 cm^{-1} corresponded to goethite (α-FeOOH), nitrate ion, and lepidocrocite (γ-FeOOH), respectively [39, 40].

The FTIR analysis results demonstrated that the prepared precursors were contained citrate-metal complexes and iron oxyhydroxide. As mentioned above, the citrate-metal ion complexes were decomposed, and metal ions were released when the temperature increases during the hydrothermal treatment. The released metal ions form metal hydroxides in the alkali medium. Therefore, when the citrate-metal ion complexes formed, hydrothermal synthesis steps were postponed and occurred at a higher temperature. One of these steps is nucleation.

Citric acid has three carboxylic acid groups in its structure. These groups can be bonded to the metal ion in different geometries, such as monodentate bonding, bidentate chelating bond, and bidentate bridging, to a form citrate-metal ion complex. Different bond geometries give rise to complexes with different geometries; for instance, 35 conformers have been identified for the zinc-citrate complex. In addition, different complex geometries have different global energy conformation and stability [41]. Different stability means, the more stable complex needed more energy to decompose. So it can be assumed that the formed complexes with C/M ratio 1 might have different geometries and higher

Fig. 2 FTIR spectra of precursors at C/M ratio (**a**) 0.5 (**b**) 1
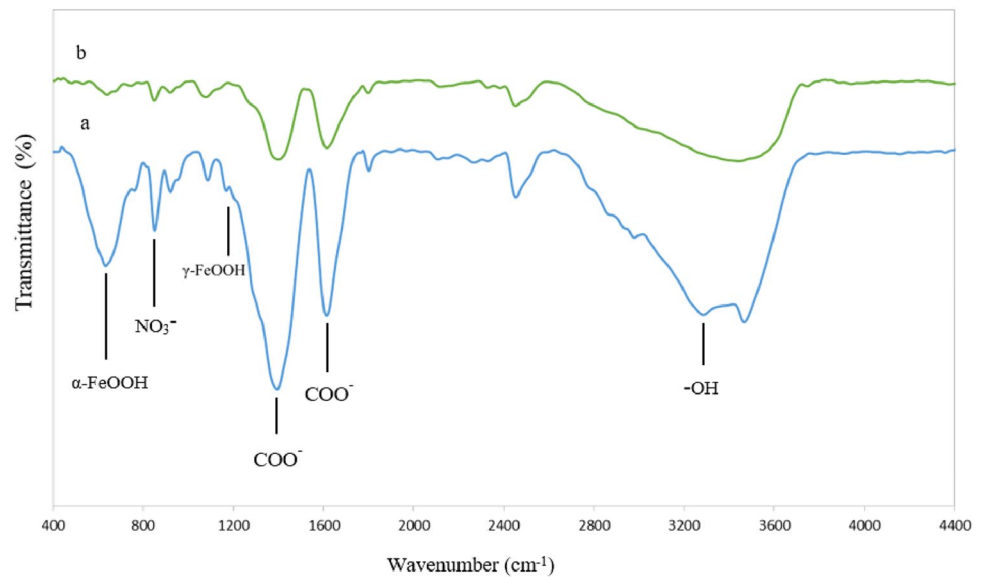
stability than those formed at 0.5 and 1.5 ratios. Complexes with higher stability decomposed at higher temperatures; thus, nucleation has occurred at the higher temperatures.

Based on the classical theory of nucleation and growth, nucleation rate (dN/dt) can be expressed as:

$$\frac{dN}{dt} = A \exp\left[-\frac{16\pi V_m^2 \gamma^3}{3k_B^3 T^3 N_A^2 (\ln S)^2}\right] \tag{2}$$

N, N_A, T, k_B, A, S, V_m, and γ are the number of nuclei, Avogadro's number, temperature, the Boltzmann constant, the pre-exponential factor, supersaturation, and surface free energy per unit area. Therefore, the nucleation rate increases exponentially when the temperature increases [42]. Stable citrate-metal ion complex formation caused that nucleation occurred at higher temperatures, and the nucleation rate increased. Increasing the nucleation rate increases the number of produced nuclei and thus decreases the size of the final crystallites.

The FESEM micrographs of the synthesized cobalt ferrite nanoparticles are presented in Fig. 3. It can be seen that as-synthesized particles had the nanometer size, uniform, narrow particle size distribution, and irregular shape. Fine particles stuck together and formed agglomerates. Furthermore, the addition of CA dramatically influenced the particle size, and the particles became finer. The sample obtained at C/M ratio 1 exhibited a smaller particle size than synthesized samples at 0.5 and 1.5. Therefore, the C/M ratio affected not only crystallite size but also particle size. Also, it seems that the synthesized particles at C/M ratio 1 show a greater tendency to agglomerate. Besides, some nanorod shape particles are also observed in the micrograph of sample CM0, as shown in Fig. 3a. These nanorods can be attributed to hematite impurities in which its trace was detected in

the XRD pattern. Furthermore, hematite nanorods synthesis using the hydrothermal method was reported [43, 44].

The magnetic hysteresis loops (*M-H*) of the synthesized nanoparticles measured at room temperature are shown in Fig. 4. The maximum magnetization (M_{max}), romance magnetization (Mr), and coercivity (Hc) values obtained from magnetic hysteresis loops are listed in Table 2. The M_{max} values were decreased from 50.3 to 40 emu/g with increasing the C/M ratio from 0.5 to 1 and then increased to 48.3 emu/g for C/M ratio 1.5. These values are lower compared to the sample prepared without CA (58.4 emu/g) and saturation magnetization value of bulk cobalt ferrite 80 emu/g [45]. Generally, cation distribution, impurity, and particle size are effective factors in the ferrite nanoparticle's magnetization. However, similar trends were observed in M_{max}, MCS, and particle size values. Therefore, the decrease in M_{max} values could be due to the particle size decreasing and the existence of spin canting layer. The disordered spin orientation or spin-canted layer exists on the surface of magnetic nanoparticles. These disordered spins lead to a decrease in the magnetization of magnetic particles. As the size of the magnetic nanoparticles decreases, the surface to volume ratio increases, and so the effect of the spin-canted layer on the total magnetization of particle increases [46].

The coercivity values have been changed from 236 to 4 Oe and then to 261 Oe by the variation of the C/M ratio from 0.5 to 1, and 1.5, respectively. Results revealed that the coercivity of nanoparticles was decreased with particle size decreasing. Generally, coercivity increases with decreasing particle size until reaching a maximum value at the single-domain critical diameter of particles. Then coercivity decreases until reaching zero in the superparamagnetic region. In the single-domain state, with the decrease in the particle size, the effect of thermal agitation becomes
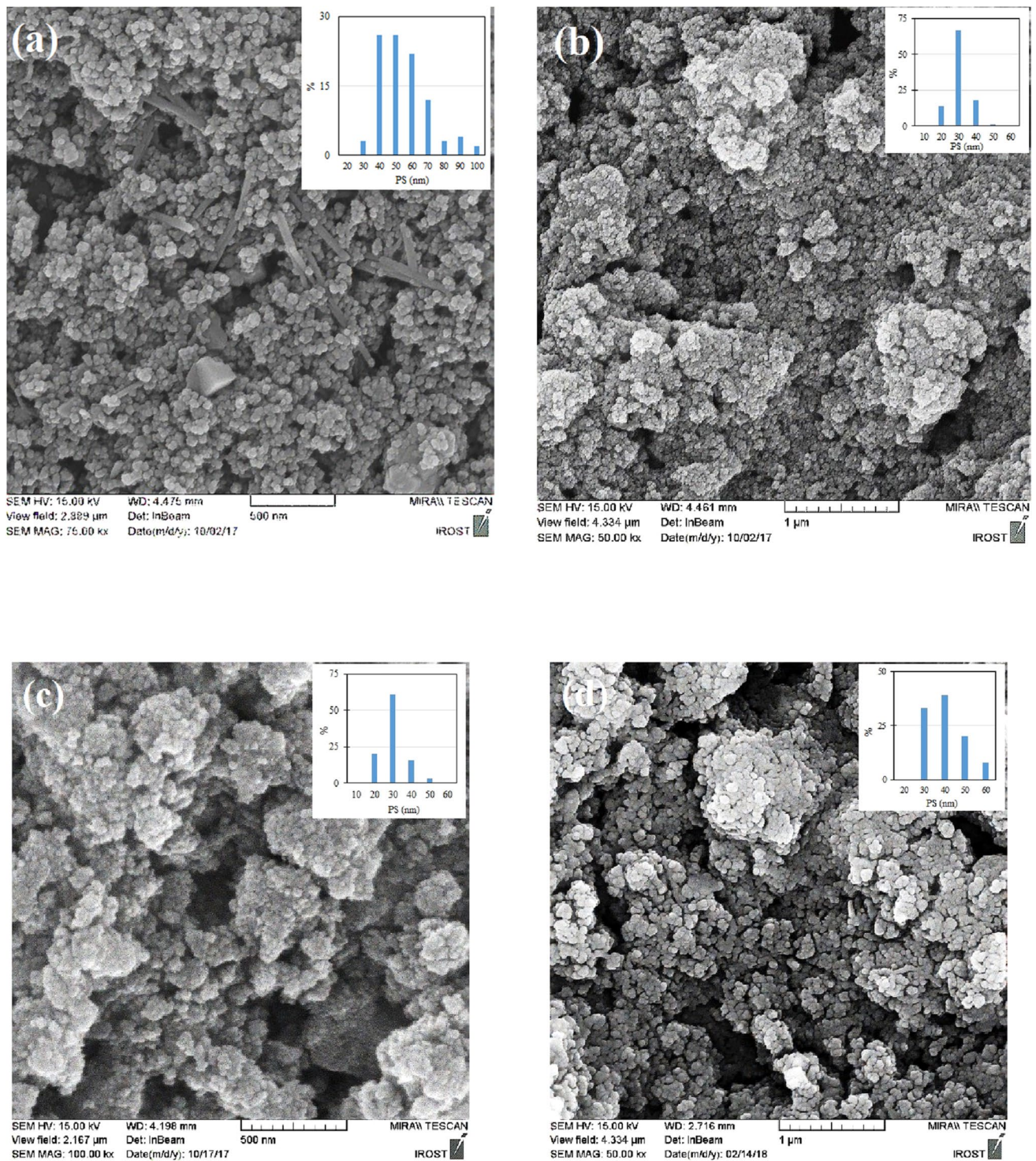
Fig. 3 FESEM micrograph of the samples (**a**) CM0, (**b**) CM0.5, (**c**) CM1, (**d**) CM1.5

more effective. Therefore, the coercivity decreases with the decrease in particle size. The single-domain critical diameter for cobalt ferrite was reported to be 40–70 nm, and related coercivity is 4650 Oe [47–49]. It can be concluded that synthesized particles are single domain, and coercivity values were decreased because of particle size decreases.

For comparison purposes, obtained results in the present research and other researches on the synthesis of cobalt
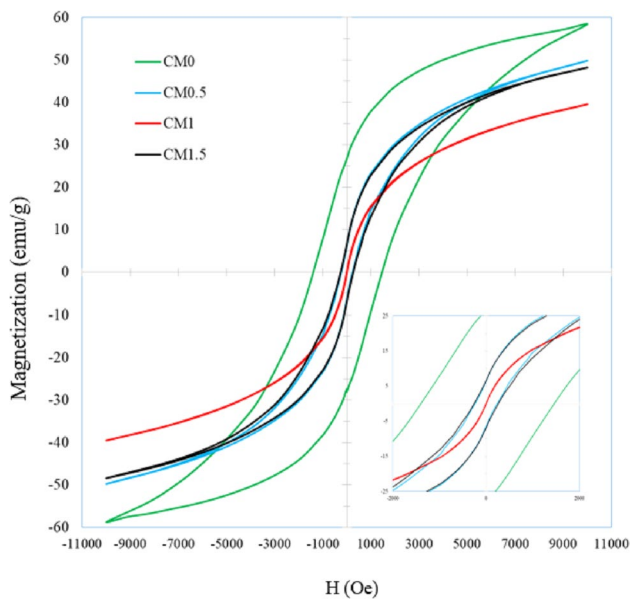
Fig. 4 VSM results of the samples

Table 2 Magnetic properties and mean crystallite size of the samples

Sample	Ms (emu/g)	Hc (Oe)	Mr (emu/g)	Mean crystallite size (nm)
CM0	58.4	1450	26.8	21.3
CM0.5	50.3	236	6.3	7.8
CM1	40	4	–	4.7
CM1.5	48.2	261	6.6	7.3

small and simple change in the concentration of citric acid, a range of properties of cobalt ferrite nanoparticles can be obtained.

4 Conclusion

In this research, the role of citric acid concentration in the hydrothermal synthesis of cobalt ferrite nanoparticles was investigated. The citric acid to the metal ion ratio (C/M) was considered as a criterion of citric acid concentration. The XRD, FE-SEM, and VSM results revealed that the mean crystallite size (MCS), particle size, and magnetic properties of synthesized nanoparticles fluctuated by the variation of the C/M ratio. The X-ray diffraction analysis exhibited that single-phase cobalt ferrite was obtained in the presence of citric acid. Besides, the crystallite size first has decreased and then increased by increasing the concentration of citric acid according to the Scherrer equation. The FE-SEM micrographs demonstrated uniform particle size distribution and irregular morphology of synthesized cobalt ferrite nanoparticles, and the citric acid concentration affects the nanoparticles' size. The FTIR spectrums of precursors revealed citrate-metal ion complexes were formed during the precursor preparation.

Moreover, cobalt ferrite nanoparticles synthesized with C/M = 0.5 exhibited Mmax value of 50 emu/g and MCS of 7.8 nm. The Mmax (40 emu/g) and MCS (4 nm) values decreased when the C/M ratio increased to 1. Further, increasing C/M to 1.5 increased Mmax (48.2 emu/g) and MCS (7.3 nm). Therefore, similar trends in particle size, MCS, and Mmax values were observed. It can be concluded that Mmax fluctuations are due to particle size variations. These changes can be due to the formation of complexes with different geometry and stability in different citric acid concentrations, which affected nucleation

ferrite by various methods are presented in Table 3. Compared to superparamagnetic nanoparticles synthesized by other methods, CF nanoparticles synthesized in C/M ratio 1 have the smallest MCS, while its Mmax is acceptable. By a

Table 3 A summary of the results obtained for cobalt ferrite nanoparticles from this research and other researches

Synthesis method	M_max (emu/g)	Hc (Oe)	Crystallite size (nm)	Reference
Coprecipitation	44.3 (20 kOe)	2	7.1	[50]
Ultrasonic-assisted solvothermal	55 (10 kOe)	–	8.3	[51]
Solvothermal	51.3 (15 kOe)	–	11	[52]
Coprecipitation	31.9 (20 kOe)	4	14.9	[53]
PVA-assisted hydrothermal	48 (14 kOe)	–	6	[54]
Hydrothermal	63.5 (50 kOe)	831	17.4	[55]
Sol–gel autocombustion	67 (12 kOe)	1215	15	[56]
Hydrothermal	58.96 (15 kOe)	289.90	10.7	[57]
Hydrothermal	46.20 (20 kOe)	870.50	53	[58]
CM0	58.4 (10 kOe)	1450	21.3	This research
CM1	40 (10 kOe)	4	4.7	This research
CM0.5	50.3 (10 kOe)	236	7.8	This research

temperature. Therefore, the particle size, crystal size, and magnetic properties are affected by the variation of the nucleation temperature and the number of created nuclei. As a result, cobalt ferrite nanoparticles with desired magnetic properties and particle size can be synthesized by adjusting the concentration of citric acid.

References

1. R. Safi, A. Ghasemi, R. Shoja-Razavi, M. Tavousi, The role of pH on the particle size and magnetic consequence of cobalt ferrite. J. Magn. Magn. Mater. **396**, 288–294 (2015)
2. A. Lu, E.L. Salabas, F. Schüth, Magnetic nanoparticles: synthesis, protection, functionalization, and application. Angew. Chemie Int. Ed. **46**(8), 1222–1244 (2007)
3. S.C.N. Tang, I.M.C. Lo, Magnetic nanoparticles: essential factors for sustainable environmental applications. Water Res. **47**(8), 2613–2632 (2013)
4. S.P. Gubin (ed.), *Magnetic Nanoparticles* (WILEY-VCH Verlag GmbH & Co KGaA, Germany, 2009)
5. S. Gyergyek, D. Makovec, A. Kodre, I. Arčon, M. Jagodič, M. Drofenik, Influence of synthesis method on structural and magnetic properties of cobalt ferrite nanoparticles. J. Nanoparticle Res. **12**(4), 1263–1273 (2010)
6. S. Jauhar, J. Kaur, A. Goyal, S. Singhal, Tuning the properties of cobalt ferrite: a road towards diverse applications. Rsc Adv. **6**(100), 97694–97719 (2016)
7. L. Ajroudi, S. Villain, V. Madigou, N. Mliki, C. Leroux, Synthesis and microstructure of cobalt ferrite nanoparticles. J. Cryst. Growth **312**(16–17), 2465–2471 (2010)
8. J.-G. Lee, J.Y. Park, C.S. Kim, Growth of ultra-fine cobalt ferrite particles by a sol–gel method and their magnetic properties. J. Mater. Sci. **33**(15), 3965–3968 (1998)
9. D.S. Mathew, R.-S. Juang, An overview of the structure and magnetism of spinel ferrite nanoparticles and their synthesis in microemulsions. Chem. Eng. J. **129**(1), 51–65 (2007)
10. J. Calvo-de la Rosa, M. Segarra, Optimization of the Synthesis of Copper Ferrite Nanoparticles by a Polymer-Assisted Sol-Gel Method. ACS Omega **4**(19), 18289–18298 (2019)
11. M. Hasheminiasari, S.M. Masoudpanah, S.M. Mirkazemi, F. Bayat, Structural and magnetic properties of ZnFe2-xInxO4 nanoparticles synthesized by solution combustion method. J. Magn. Magn. Mater. **442**, 468–473 (2017)
12. S. Zhang, Q. Jiao, Y. Zhao, H. Li, Q. Wu, Preparation of rugby-shaped CoFe 2 O 4 particles and their microwave absorbing properties. J. Mater. Chem. A **2**(42), 18033–18039 (2014)
13. V. Pillai, D.O. Shah, Synthesis of high-coercivity cobalt ferrite particles using water-in-oil microemulsions. J. Magn. Magn. Mater. **163**(1–2), 243–248 (1996)
14. I.H. Gul, A. Maqsood, M. Naeem, M.N. Ashiq, Optical, magnetic and electrical investigation of cobalt ferrite nanoparticles synthesized by co-precipitation route. J. Alloys Compd. **507**(1), 201–206 (2010)
15. E. Mazario, M.P. Morales, R. Galindo, P. Herrasti, N. Menendez, Influence of the temperature in the electrochemical synthesis of cobalt ferrites nanoparticles. J. Alloys Compd. **536**, S222–S225 (2012)
16. L. Pérez-Mirabet et al., One-pot synthesis of stable colloidal solutions of MFe2O4 nanoparticles using oleylamine as solvent and stabilizer. Mater. Res. Bull. **48**(3), 966–972 (2013)
17. M. Sajjia, M. Oubaha, M. Hasanuzzaman, A.G. Olabi, Developments of cobalt ferrite nanoparticles prepared by the sol–gel process. Ceram. Int. **40**(1), 1147–1154 (2014)
18. S. Jovanović, M. Spreitzer, M. Otoničar, J.-H. Jeon, D. Suvorov, pH control of magnetic properties in precipitation-hydrothermal-derived CoFe2O4. J. Alloys Compd. **589**, 271–277 (2014)
19. I. Ibrahim, I.O. Ali, T.M. Salama, A.A. Bahgat, M.M. Mohamed, Synthesis of magnetically recyclable spinel ferrite (MFe2O4, M=Zn Co, Mn) nanocrystals engineered by sol gel-hydrothermal technology: High catalytic performances for nitroarenes reduction. Appl. Catal. B Environ. **181**, 389–402 (2016)
20. M. Yoshimura, K. Byrappa, Hydrothermal processing of materials: past, present and future. J. Mater. Sci. **43**(7), 2085–2103 (2008)
21. J. Ortiz-Landeros, C. Gómez-Yáñez, R. López-Juárez, I. Dávalos-Velasco, H. Pfeiffer, Synthesis of advanced ceramics by hydrothermal crystallization and modified related methods. J. Adv. Ceram. **1**(3), 204–220 (2012)
22. L. Yao, Y. Xi, G. Xi, Y. Feng, Synthesis of cobalt ferrite with enhanced magnetostriction properties by the sol− gel− hydrothermal route using spent Li-ion battery. J. Alloys Compd. **680**, 73–79 (2016)
23. M. Jalalian, S.M. Mirkazemi, S. Alamolhoda, The effect of poly vinyl alcohol (PVA) surfactant on phase formation and magnetic properties of hydrothermally synthesized CoFe2O4 nanoparticles. J. Magn. Magn. Mater. **419**, 363–367 (2016)
24. G.B. Ji, S.L. Tang, S.K. Ren, F.M. Zhang, B.X. Gu, Y.W. Du, Simplified synthesis of single-crystalline magnetic CoFe2O4 nanorods by a surfactant-assisted hydrothermal process. J. Cryst. Growth **270**(1–2), 156–161 (2004)
25. T. Jiang et al., Citric acid-assisted hydrothermal synthesis of α-NaYF 4: Yb 3+, Tm 3+ nanocrystals and their enhanced ultraviolet upconversion emissions. CrystEngComm **14**(6), 2302–2307 (2012)
26. W. Di, M.-G. Willinger, R.A.S. Ferreira, X. Ren, S. Lu, N. Pinna, Citric acid-assisted hydrothermal synthesis of luminescent TbPO4: Eu nanocrystals: controlled morphology and tunable emission. J. Phys. Chem. C **112**(48), 18815–18820 (2008)
27. S. Cho, J.-W. Jang, S.-H. Jung, B.R. Lee, E. Oh, K.-H. Lee, Precursor effects of citric acid and citrates on ZnO crystal formation. Langmuir **25**(6), 3825–3831 (2009)
28. M. Zahraei, A. Monshi, M. del Puerto Morales, D. Shahbazi-Gahrouei, M. Amirnasr, B. Behdadfar, Hydrothermal synthesis of fine stabilized superparamagnetic nanoparticles of Zn2+ substituted manganese ferrite. J. Magn. Magn. Mater. **393**, 429–436 (2015)
29. B. Behdadfar, A. Kermanpur, H. Sadeghi-Aliabadi, M. del Puerto Morales, M. Mozaffari, Synthesis of aqueous ferrofluids of ZnxFe3− xO4 nanoparticles by citric acid assisted hydrothermal-reduction route for magnetic hyperthermia applications. J. Magn. Magn. Mater. **324**(14), 2211–2217 (2012)
30. M. Saini, B.S. Dehiya, A. Umar, M.S. Goyat, Phase modulation in nanocrystalline vanadium di-oxide (VO2) nanostructures using citric acid via one pot hydrothermal method. Ceram. Int. **45**(15), 18452–18461 (2019)
31. S.-M. Park, C. Nam, Dye-adsorption properties of WO3 nanorods grown by citric acid assisted hydrothermal methods. Ceram. Int. **43**(18), 17022–17025 (2017)
32. J.I. Langford, A.J.C. Wilson, Scherrer after sixty years: a survey and some new results in the determination of crystallite size. J. Appl. Crystallogr. **11**(2), 102–113 (1978)
33. D.W. Barnum, Hydrolysis of cations. Formation constants and standard free energies of formation of hydroxy complexes. Inorg. Chem. **22**(16), 2297–2305 (1983)
34. A.E. Danks, S.R. Hall, Z. Schnepp, The evolution of 'sol–gel' chemistry as a technique for materials synthesis. Mater. Horizons **3**(2), 91–112 (2016)

35. X. Zhao, F. Lou, M. Li, X. Lou, Z. Li, J. Zhou, Sol− gel-based hydrothermal method for the synthesis of 3D flower-like ZnO microstructures composed of nanosheets for photocatalytic applications. Ceram. Int. **40**(4), 5507–5514 (2014)

36. X. Zhao, M. Li, X. Lou, Sol–gel assisted hydrothermal synthesis of ZnO microstructures: morphology control and photocatalytic activity. Adv. Powder Technol. **25**(1), 372–378 (2014)

37. I.A.F. de Medeiros, A.L. Lopes-Moriyama, C.P. de Souza, Effect of synthesis parameters on the size of cobalt ferrite crystallite. Ceram. Int. **43**(5), 3962–3969 (2017)

38. Z. Chen, J. Hu, Z. Lu, X. He, Low-temperature preparation of lanthanum-doped BiFeO 3 crystallites by a sol–gel-hydrothermal method. Ceram. Int. **37**(7), 2359–2364 (2011)

39. L. Shi, Y. Tan, N. Tsubaki, A solid-state combustion method towards metallic Cu–ZnO catalyst without further reduction and its application to low-temperature methanol synthesis. ChemCatChem **4**(6), 863–871 (2012)

40. G.S.R. Krishnamurti, P.M. Huang, Influence of citrate on the kinetics of Fe (II) oxidation and the formation of iron oxyhydroxides. Clays Clay Miner. **39**(1), 28–34 (1991)

41. C.C.R. Sutton, G. da Silva, G.V. Franks, Bonding of aqueous citrate with Zn2+ and ZnO nanoclusters: a theoretical study. ChemistrySelect **2**(6), 2055–2064 (2017)

42. S.G. Kwon, T. Hyeon, Formation mechanisms of uniform nanocrystals via hot-injection and heat-up methods. Small **7**(19), 2685–2702 (2011)

43. C. Jia et al., Single-crystalline iron oxide nanotubes. Angew. Chemie **117**(28), 4402–4407 (2005)

44. Z. Li, X. Lai, H. Wang, D. Mao, C. Xing, D. Wang, Direct hydrothermal synthesis of single-crystalline hematite nanorods assisted by 1, 2-propanediamine. Nanotechnology **20**(24), 245603 (2009)

45. U. Kurtan, R. Topkaya, A. Baykal, M.S. Toprak, Temperature dependent magnetic properties of CoFe2O4/CTAB nanocomposite synthesized by sol–gel auto-combustion technique. Ceram. Int. **39**(6), 6551–6558 (2013)

46. B. Issa, I.M. Obaidat, B.A. Albiss, Y. Haik, Magnetic nanoparticles: surface effects and properties related to biomedicine applications. Int. J. Mol. Sci. **14**(11), 21266–21305 (2013)

47. C.N. Chinnasamy et al., Unusually high coercivity and critical single-domain size of nearly monodispersed CoFe 2 O 4 nanoparticles. Appl. Phys. Lett. **83**(14), 2862–2864 (2003)

48. L. Zhao et al., Studies on the magnetism of cobalt ferrite nanocrystals synthesized by hydrothermal method. J. Solid State Chem. **181**(2), 245–252 (2008)

49. D.L. Leslie-Pelecky, R.D. Rieke, Magnetic properties of nanostructured materials. Chem. Mater. **8**(8), 1770–1783 (1996)

50. O. Karaagac, B.B. Yildiz, H. Köçkar, The influence of synthesis parameters on one-step synthesized superparamagnetic cobalt ferrite nanoparticles with high saturation magnetization. J. Magn. Magn. Mater. **473**, 262–267 (2019)

51. A.R. Abbasian, Z. Lorfasaei, M. Shayesteh, M.S. Afarani, Synthesis of cobalt ferrite colloidal nanoparticle clusters by ultrasonic-assisted solvothermal process. J. Aust. Ceram. Soc. **56**(3), 1119–1126 (2020)

52. B. Thomas, L.K. Alexander, Enhanced synergetic effect of Cr (VI) ion removal and anionic dye degradation with superparamagnetic cobalt ferrite meso–macroporous nanospheres. Appl. Nanosci. **8**(1–2), 125–135 (2018)

53. O. Karaagac, B. Bilir, H. Kockar, Superparamagnetic cobalt ferrite nanoparticles: effect of temperature and base concentration. J. Supercond. Nov. Magn. **28**(3), 1021–1027 (2015)

54. M. Jalalian, S.M. Mirkazemi, S. Alamolhoda, Phase constituents and magnetic properties of the CoFe 2 O 4 nanoparticles prepared by polyvinylpyrrolidone (PVP)-assisted hydrothermal route. Appl. Phys. A **122**(9), 835 (2016)

55. Y. Köseoğlu, F. Alan, M. Tan, R. Yilgin, M. Öztürk, Low temperature hydrothermal synthesis and characterization of Mn doped cobalt ferrite nanoparticles. Ceram. Int. **38**(5), 3625–3634 (2012)

56. B.G. Toksha, S.E. Shirsath, S.M. Patange, K.M. Jadhav, Structural investigations and magnetic properties of cobalt ferrite nanoparticles prepared by sol–gel auto combustion method. Solid State Commun. **147**(11–12), 479–483 (2008)

57. S. Fayazzadeh, M. Khodaei, M. Arani, S.R. Mahdavi, T. Nizamov, A. Majouga, Magnetic properties and magnetic hyperthermia of cobalt ferrite nanoparticles synthesized by hydrothermal method. J. Supercond. Nov. Magn. **33**(7), 2227–2233 (2020)

58. M. Bououdina, C. Manoharan, Dependence of structure/morphology on electrical/magnetic properties of hydrothermally synthesised cobalt ferrite nanoparticles. J. Magn. Magn. Mater. **493**, 165703 (2020)